Materials Science Forum
ISSN: 1662-9752, Vol. 1182, pp 135-146
doi:10.4028/p-hZfPy4

Submitted: 2026-01-19
Revised: 2026-02-16
Accepted: 2026-02-17
Online: 2026-04-10

A Unified Simulation Environment for Thermoforming and Distortion Prediction of CFRTP Aircraft Components

Miro Duhovica[1,a*], Lukas Handl[1,b], Martin Müller[1,c], Dominic Schommer[1,d], Thomas Hoffmann[1,e], Jens Schlimbach[1,f], Thomas Neumeyer[1,g]

[1]Leibniz-Institut für Verbundwerkstoffe GmbH, Erwin-Schrödinger-Straße 58, 67663 Kaiserslautern, Germany

[a]Miro.Duhovic@leibniz-ivw.de, [b]Lukas.Handl@leibniz-ivw.de, [c]Martin.Mueller@leibniz-ivw.de, [d]Dominic.Schommer@leibniz-ivw.de, [e]Thomas.Hoffmann@leibniz-ivw.de, [f]Jens.Schlimbach@leibniz-ivw.de, [g]Thomas.Neumeyer@leibniz-ivw.de

*corresponding author

Keywords: process simulation, thermoforming, spring-angle prediction, digital process chain.

Abstract. This paper presents a comprehensive fully integrated polymer composite thermoforming process simulation chain developed in ANSYS LS-DYNA®, covering the full manufacturing sequence from automated preform creation to final part cooling. The entire simulation consists of three distinct phases, namely, thermoforming, cooling (within the tool) and manufacturing-induced dimensional distortion after demolding (spring-back), where distortions develop as the part is removed from the tooling and finally cools to room temperature. The simulation framework employs a modular model structure consisting of tooling, a preform holding system, and a detailed preform representation based on a semi-discrete unit cell approach. Individual laminate plies are modeled using a combination of beam, solid, and shell elements and simple material models to accurately capture temperature-dependent bending, shear, and thermal behavior of the preform. To ensure industrial applicability, an automated preform meshing strategy has also been developed, utilizing tape placement path planning data exported from the automated tape laying process to generate simulation models with minimal manual effort. The simulation results enable the prediction of spring-angle distortions (spring-in or spring-back) and can be validated against experimental distortion measurement data from manufacturing trials of several different representative CFRTP components. The presented approach demonstrates the capability of the newly developed simulation chain to support thermoforming process development, tool geometry compensation, and robust manufacturing of complex thermoformed CFRTP structures.

Introduction

The absence of efficient manufacturing routes for fiber-reinforced thermoplastics (FRTPs) has led to the continued use of aluminum or labor-intensive thermoset-based construction methods for the manufacture of structural aerospace components. Within several German Federal Aviation Research projects, the Leibniz-Institut für Verbundwerkstoffe GmbH (Leibniz Institute for Composite Materials) and its project partners have been developing an efficient process chain for the cost-effective production of complex carbon fiber-reinforced thermoplastic components (CFRTPs). This effort combines the key processes of automated tape laying/placement (ATL/ATP), thermoforming, co-consolidation, and over-molding. In this manufacturing route, unidirectional tapes are first converted into customized, material-efficient 2D preforms using a high-speed multiaxial tape-laying machine. Both straight and curved fiber paths can be produced in-line with the part's load bearing directions. Using the thermoforming process, these 2D preforms are reshaped into their final 3D geometry. The preform is first heated by IR-radiation to temperatures above 400 °C depending on the polymer to achieve drapeability and is then formed into the desired shape using a press equipped with the corresponding matched die tooling [1]. More complex integrated structures can be achieved through additional over-molding via injection molding channels and cavities or joining steps via co-consolidation functionality. This process chain offers numerous advantages, including high

production rate, fully integrated manufacturing structural components from hybrid materials, a high degree of automation, and improved damage tolerance. In addition, the inherent weldability of thermoplastics enables the efficient joining of additional parts and repair of components, while recyclability provides a clear advantage over thermosets. However, during the manufacture of such complexly curved or angled CFRTP components, undesirable component deformations and distortions may occur, particularly during thermoforming at high processing temperatures, cooling within the tool, and further cooling of the part to its working temperature. These deformations can pose major challenges during subsequent assembly processes. To support the development of parts produced using this manufacturing process, CAE tools such as finite element simulations are used to model the entire process chain, predict distortion effects, and adjust the required tool geometry accordingly to compensate for these effects. This minimizes the need for costly production trials, tool rework, and the trial-and-error determination of optimal process parameters.

State of the Art

Thermoforming.

The thermoforming of fiber-reinforced thermoplastics is a highly efficient manufacturing process that leverages the ability of thermoplastic polymers to soften and become moldable when heated, and to solidify again upon cooling. Unlike thermosetting composites, this reversible phase change enables very short cycle times and the use of forming techniques similar to those used in metalworking [2, 3]. Thermoforming describes the reshaping of flat, pre-consolidated laminate structures (also known as preforms) into complex two- or three-dimensional components under the influence of heat and pressure. An essential factor in the processing of continuous fiber-reinforced thermoplastics is that the reinforcing fibers (in particular carbon fibers) are practically inextensible during forming. Therefore, the matrix must be molten during deformation to enable deformation processes such as inter-ply slip and intra-ply shear to occur, allowing the fibers to conform to the tool geometry without kinking or breaking [2, 4]. The process is often performed using stamp forming in a mechanical or hydraulic press. In the considered process chain, tailored preforms are first produced using the ATP or ATL method. Individual ply layers with the desired fiber orientation are laid down using pre-consolidated preform laminate [1, 2]. However, other types of preforms can also be used, such as fabric fiber-reinforced preforms, film stacked prepregs, or commingled yarns [2]. The preform is then heated in an external heating device (e.g., by contact heat, infrared radiation, or convection) above melt temperature, T_m for semi-crystalline polymers or well above the glass transition temperature, T_g for amorphous polymers. In this state, the material is flexible and deformable. The hot laminate is then quickly transferred (within a few seconds) to the forming tool to prevent premature cooling. Once positioned in the tool, the press closes and shapes the preform by pressing it between the tool cavities. The component cools under pressure within the tool to well below T_m or T_g. Once a uniform temperature is reached and any recrystallization effects have occurred, the finished part is removed from the tool [1, 2, 4]. When thermoforming CFRTP components, undesired deviations from the intended part geometry often arise during cooling. Components with curvature or angled surfaces are particularly prone to these distortions [5, 6]. These distortions are usually due to internal stress states caused by the forces involved in the thermoforming process, differences in thermal expansion of the reinforcing fibers and polymer matrix, crystallization effects and the anisotropic properties of CFRTP laminates [3, 5]. As a result, two main phenomena are observed: spring-in and spring-back. The extent of each effect is influenced by the material combination (fiber types/reinforcing structures and polymer), processing parameters and the component design. An overview of these parameters and some general trends indicating the potential impact on distortion (spring-angle) behavior is presented in Table 1. Detailed modeling of the entire process chain has already been demonstrated in the physics-based virtual-twin stamp-forming simulation workflow of Pipes [7].In many current approaches, including that of Pipes, the forming simulation and the subsequent distortion (spring-angle) simulation are often carried out in two separate simulation/software environments.

This can make it challenging to fully carry over the process-induced forces and stress states from the forming phase into the distortion simulation.

Table 1. General trends in the influence of processing parameters and component design on spring-angle distortion, according to [1, 2, 3, 4, 5, 6, 8, 9, 11].

Parameter		Spring-Angle Δϕ	Explanation	
			Spring-In 	**Spring-Back** 
Processing temperature ***T***		***T*↗** **Δϕ ↘**	Spring-in is proportional to the temperature difference between processing temperature and ambient temperature after demolding [4].	Higher tool and component temperatures reduce spring-back, as improved matrix flow and reduced material elasticity decrease stress build-up [9].
Press force ***F***		***F*↗** **Δϕ ↘ / ↗**	Higher tool pressure leads to stronger transverse matrix flow and increased fiber waviness, which can result in smaller end angles in bending zones [6, 9].	Higher pressing force leads to greater spring-back due to higher residual stress caused by stretching of the molecular chains [1, 2].
Closing velocity ***v***		***v*↗** **Δϕ →**	High velocity is necessary to maintain the laminate temperature above the critical level required for inter-ply slip and kink-free shaping [1, 4].	-
Holding time ***t***		***t*↗** **ϕ →**	Longer holding times allow the matrix to fix the fibers more firmly during cooling, which reduces the elastic recovery (spring-back) of the fibers and results in a more consistent and uniform final angle [1, 2].	Longer holding time reduces spring-back, as the matrix has more time to solidify and fix bent fibers in place [1, 2].
Laminate thickness ***d***		***d*↗** **Δϕ →**	Thinner components tend to exhibit more spring-in than thicker ones. Measurements on L-profiles showed a 64% higher spring-in rate for 1 mm laminates compared to 12 mm laminates [6, 9].	Very thin laminates (1–3 layers) exhibit spring-back due to low stiffness against residual stresses [9].
Laminate structure	Change from UD to quasiisotropic	**Δϕ ↘**	Quasi-isotropic laminates exhibit greater spring-in than UD laminates due to the stronger Poisson effect and the resulting contraction in the thickness direction [6].	-
	Fabric instead of UD Tape	**Δϕ ↗**	No spring-in effect observed	Fabric-reinforced laminates tend to cause spring-back [2], [10].
Form radius ***r***		***r*↗** **Δϕ →**	Studies suggest that radius size has only a minor influence [2, 6].	Spring-back decreases with increasing mold radius, as local deformation becomes less pronounced [2, 4].
Flange length ***l***		***l*↗** **Δϕ ↘**	Measured total deformation increases with the length of the flat sections, especially in thin laminates. This is largely due to the distortion of the flat sections [6].	-

The simulation framework developed here provides a unified environment that enables the study of the influence of all important parameters throughout the entire thermoforming process chain. In the current implementation, strain-rate and cooling-rate effects have not yet been included, as simplified material models were used initially; however, more sophisticated models can be incorporated in future enhancements. In addition, the material models account for volume changes due to both thermal expansion and crystallization through a temperature-dependent "crystallinity-adjusted" thermal expansion coefficient.

Spring-In-Effect.

The spring-in effect (also known as the spring-forward phenomenon) is a phenomenon of shape distortion that can occur during thermoforming at high processing temperatures of angular or curved CFRTP components [5, 6]. It manifests itself in the reduction of the included angle of a molded component when it cools from processing temperature to operating temperature. The main cause of this phenomenon is the anisotropy of the thermal properties of fiber-reinforced composites. The thermal out-of-plane expansion coefficient (radial) is significantly higher than in the in-plane direction (tangential). This situation arises because the carbon fibers have an extremely low (close to zero) coefficient of thermal expansion (CTE) in the fiber direction, while the matrix has a comparatively much higher CTE. This causes the material to contract more in the thickness direction than in the fiber direction, causing the two curved sides to move closer together due to the greater contraction in the thickness direction, thus increasing the sector angle, which leads to a reduction in the enclosed angle [1, 2, 3, 4]. Studies have shown that partially crystalline thermoplastic matrices undergo anisotropic thermophysical phase-change shrinkage during crystallization, which promotes the spring-forward effect; additionally, in semi-crystalline thermoplastics, the glass transition temperature may be crossed during cooling, leading to a pronounced change in the coefficient of thermal expansion [6, 7]. In addition to material anisotropy, other mechanisms also contribute to this phenomenon. For example, the complexity of the component also plays a significant role. In complex geometries, such as a "top hat" component, the inherent boundary conditions lead to stress build-up and additional warping, such as the dishing effect and curving of the flat base [3, 6]. Furthermore, during thermoforming, the wrinkling of the fiber bundles in the bending area can contribute to a reduction in the end angle, especially if the pressure leads to axial compression of the fibers [1, 2, 8]. In addition, thickness reductions due to transverse matrix flow or resin percolation can also influence the end angle and depend on the laminate structure [1].

Spring-Back-Effect.

The spring-back effect (also known as spring-backward) in thermoforming CFRTPs describes the increase in angle in a curved component after cooling from the processing temperature to the usage temperature [2, 4, 9]. In general, the spring-back effect occurs less frequently in the thermoforming of CFRTPs than the spring-in effect described above, as the deformations resulting from thermal anisotropy often predominate [9]. Typically, the effect is observed primarily in fabric-reinforced laminates compared to unidirectional tapes, which often exhibit spring-in [2, 4]. One of the main causes is residual mechanical stress in the laminate. When the laminate is formed, elastic energy is stored in the fibers, which causes the component to spring-back to its original shape after it is removed from the tool [2]. The effect is also enhanced by the residual yield strength present even at high temperatures, which leads to elastic recovery of the material [8, 9]. Spring-back can also occur as recovery after initial spring-in. The viscoelastic recovery of the matrix over a long period of time (up to three years) causes molecular rearrangement, which in turn leads to the release of residual stresses [12].

Methodology

To provide computer-aided support and optimization for the CFRTP manufacturing process chain described above, a methodology was developed in ANSYS LS-DYNA® that simulates the entire thermoforming process, from tape-laying to final forming. The simulation model consists of three

main components: the preform, the preform holder system, and the tooling. These components were developed modularly to ensure a high degree of flexibility, allowing, for example, different tool cavities or preforms with varying properties and geometries to be easily interchanged within the model. The process chain is divided into five steps (two model generation steps and three simulation phases), each representing a different stage of the process supporting real-world operations. A complete overview of the simulated process chain is shown in Fig. 1.

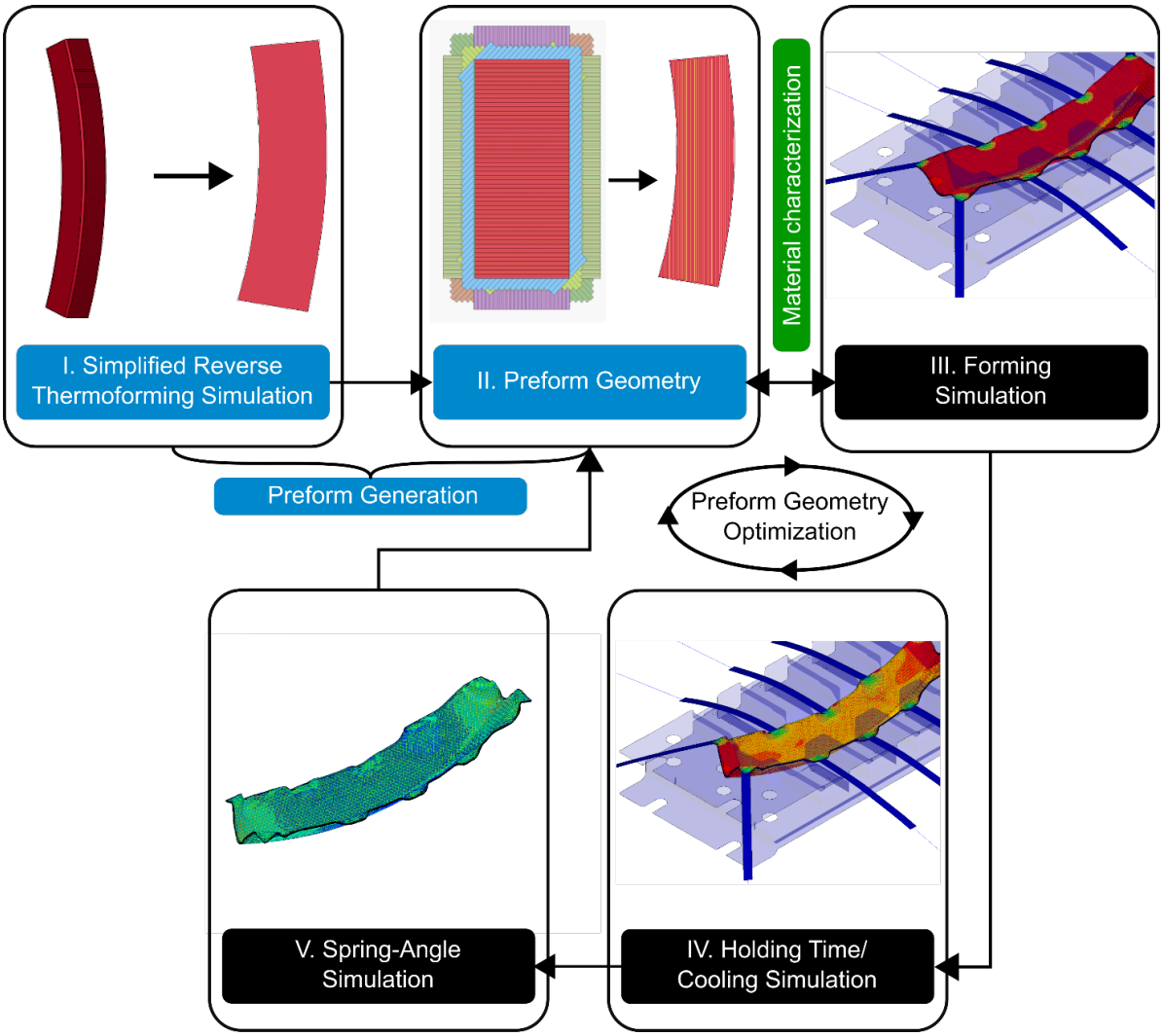

Fig. 1. Flowchart of the simulated process chain, where the first two steps correspond to preform generation and the remaining three steps represent the actual simulation phases.

Reverse Thermoforming Simulation.

The first step in the simulation process chain does not correspond to an actual manufacturing operation but serves to support the planning of preform production using the ATP/ATL method. This helps minimize costly and time-consuming trial-and-error procedures required to generate a geometry suitable for later manufacturing via ATP/ATL. LS-DYNA® includes a feature that allows simple profiles to be converted into a flat component through a simplified reverse forming simulation, which still preserves the outer contour of the original part. This reverse forming simulation requires minimal input data. A 3D model of the component, in a common CAD format such as ".STEP," is loaded into LS-PrePost as the input file. An automated meshing tool is then used to generate a shell mesh on the outer surface, and the material behavior can be assigned from a predefined selection of material data. With minimal computational effort and processing time, the software converts the 3D part shape into a flattened preform mesh geometry (see Fig. 1 I.). The resulting boundary of the mesh can then be converted into a geometric format such as ".IGES", which is then used as input for programming the tape-laying machine.

Preform Generation.

To capture the complex deformation behavior of CFRTPs during thermoforming, a semi-discrete solid mechanics approach based on the unit cell concept of Duhovic and Schommer [13] is used to model the preform (see Fig. 2). Instead of representing an incremental section with a single element type, the deformation behavior is modeled through a combination of interacting elements within the so-called unit cell. Beam, shell, and solid elements are employed for this purpose. Beam elements capture fiber orientation and define the bending stiffness of each layer, while solid elements define shear stiffness. Shell elements, also referred to as "null elements", do not possess any mechanical properties but serve to establish thermal contact between the beam and solid elements. Each ply of the laminate is modeled individually using this three-element approach, with individual plies connected to one another via sliding contact conditions. *MAT_ELASTIC_PLASTIC_THERMAL and *MAT_THERMO_ELASTO_VISCO _PLASTIC_CREEP are applied to the beam and solid elements, respectively. The former assigns temperature-dependent values for stiffness, Poisson's ratio, thermal expansion coefficient, yield stress, and tangent modulus to the beam elements representing the fiber behavior. The latter enables the definition of temperature-dependent stress–strain curves and a temperature-dependent thermal expansion coefficient assigned to the solid elements representing the polymer behavior. Additionally, an averaged, temperature-independent, Coulomb-based contact friction is applied between the laminate plies during the thermoforming phase, which is then locked during the subsequent holding and cooling phases (Figure 1 IV and V). The same constitutive models are applied throughout all simulation phases. Therefore, the above-mentioned material properties must be available over a broad temperature range, from the forming process down to room temperature.

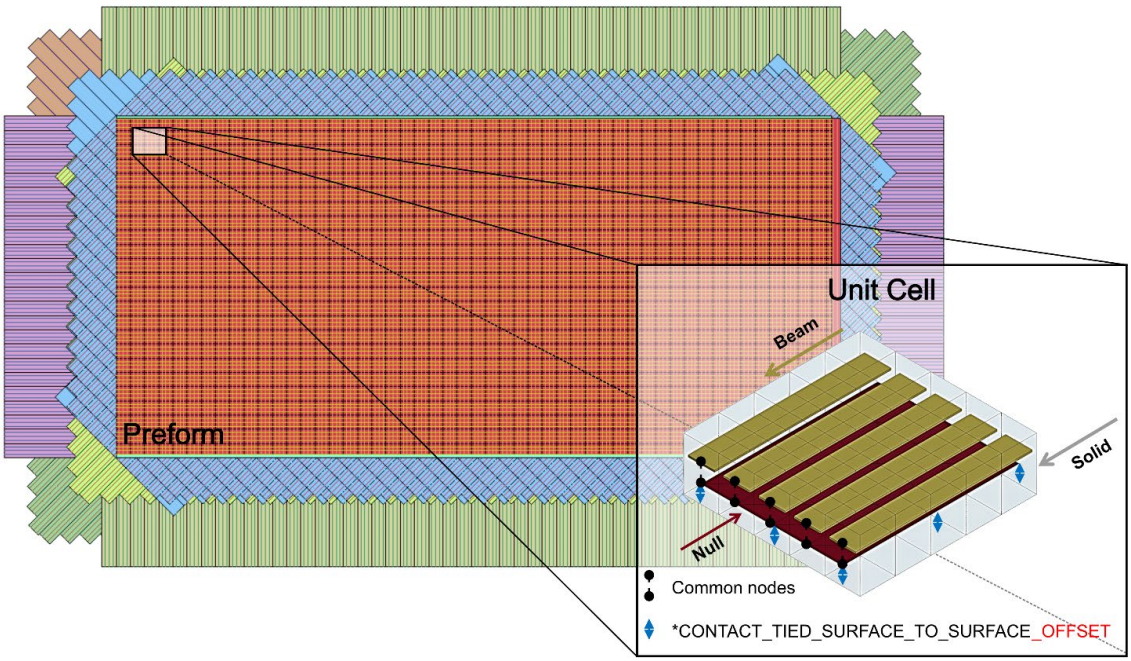

Fig. 2. Preform generated in LS-PrePost and the corresponding unit cell concept.

As a result, forming induced fiber stresses are included in the shape-distortion predictions. The required material model parameters can be obtained from material property data sheets and the characterization tests shown in Figure 3.

Since generating the preform mesh is labor-intensive, an automated meshing technique has been developed. A JSON file from the multiaxial tape-laying machine, which contains the exact planned placement paths of the preform tapes, is used by a Python script to generate macros that are later imported into LS-PrePost® to construct the mesh along the correct paths, following the unit cell modeling approach described above. The beam elements are precisely aligned with the tape-laying

direction, corresponding to the fiber orientation. Solid elements are generated along the placement paths and across the tape width, with adjustable element sizes to allow increased mesh resolution and simulation accuracy — albeit at the cost of longer computation times. Null elements are defined per layer based on the nodal points generated by the beam elements. The complete preform mesh is then assembled layer by layer according to this principle. A preform created using this method is shown in Fig 2. Once generated, the mesh can be trimmed to the desired final contour using the specified geometry data (see Fig. 1 II). Contact conditions within each unit cell, as well as between individual layers, are automatically established by the script. After all model components including the preform, the preform holder system and the tooling are assembled in 3D space, process parameters can be defined using the appropriate keywords and boundary conditions.

Material Characterization.

The forming and draping behavior of the preform is defined using standard material models already available within LS-DYNA®. For this purpose, the bending and shear behavior over the relevant processing temperature range was experimentally characterized.

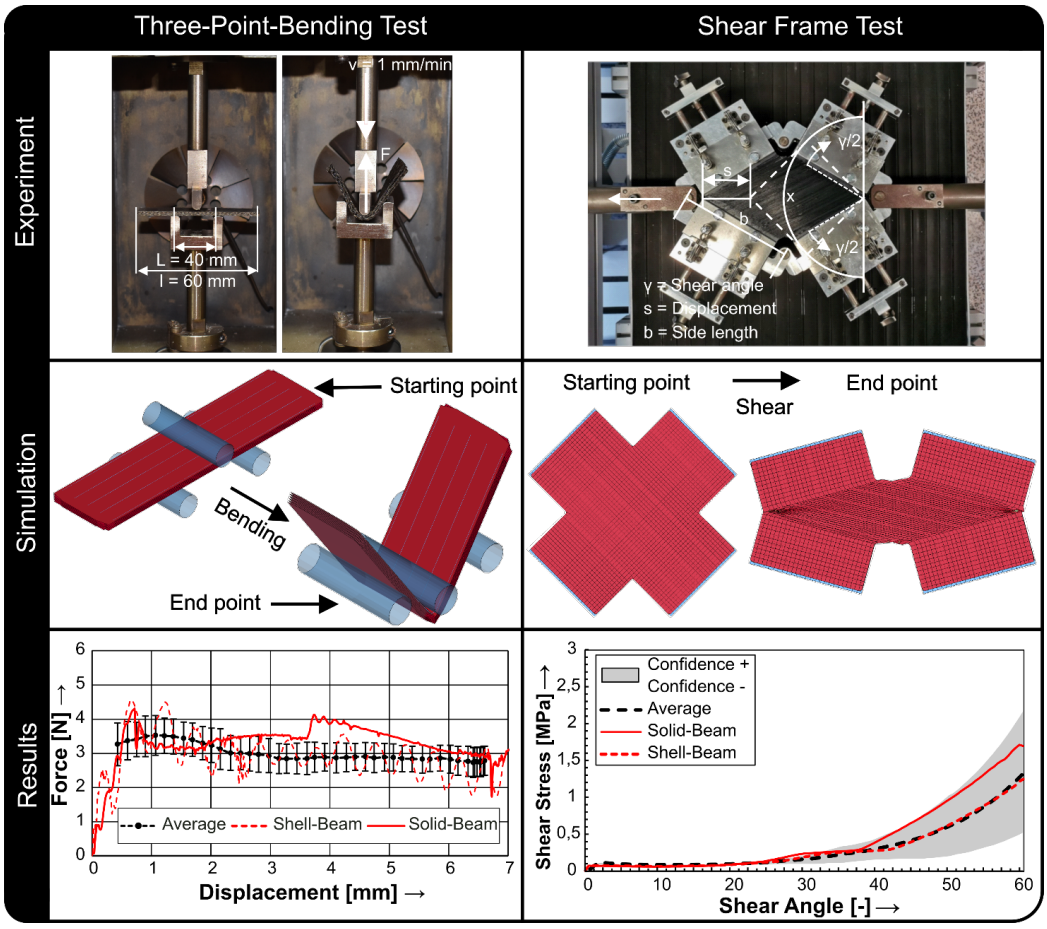

Fig. 3. Processing temperature material characterization using three-point bending and shear frame test.

The characterization data presented in Fig. 3 were obtained for the high-performance carbon-fiber-reinforced thermoplastic polymer LM PAEK (TC1225) from Toray. Temperature-dependent three-point bending and shear-frame tests were conducted-typically at a minimum of three temperatures within the recommended forming range, with at least five repetitions at each temperature-to determine the corresponding stiffness values. These experiments were then reproduced numerically, and the bending and shear stiffness parameters were iteratively calibrated until good agreement with the experimental results was achieved. Additional preform material properties, including the temperature-dependent coefficient of thermal expansion (CTE), thermal conductivity, and heat capacity, were taken from the material data sheets.

Forming Simulation.

This step represents the first of three stages of the thermoforming process. Initially, a structured master model is generated, consisting of three primary components: the tool cavity, the preform holder, and the preform described in the preceding simulation step. The modular design of the overall model enables the straightforward exchange of different tools and preforms, as well as the efficient adjustment of process parameters with minimal modeling effort. The tool is represented solely by the tool cavities using a shell mesh and is assumed to behave as a rigid body. The preform is positioned centrally between the upper and lower tool and is accurately aligned within the plane. In accordance with the real manufacturing setup, positioning is achieved using aluminum strips and holding springs/wires. The aluminum strips are also modeled using shell elements and are connected to the preform via tied contact definitions on the preform side. At their opposite ends, the springs/wires are represented by appropriate boundary conditions, which are fixed either in space or to a corresponding frame. The initial state of the simulation corresponds to a preform that has already been heated above the glass transition temperature and positioned correctly within the open tool. Accordingly, both the preform and the tool are assigned initial temperatures reflecting the actual thermal conditions at this stage of the process. In this model, the temperature distribution within the tool is assumed to be homogeneous and remains constant throughout the simulation. However, non-uniform steady-state temperature distributions can also be prescribed and simulated. Upon initiation of the simulation, the tool begins to close and presses the preform into the tool cavity. The closing movement can be controlled either by a prescribed motion, defined by a target gap width, or by a force-controlled approach until a specified maximum forming force is reached. In both cases, the motion is governed by a smooth curve in time. From the onset of the simulation, the preform cools via free convection to the surrounding air, which is defined through appropriate thermal boundary conditions. Once contact between the tool and the preform is established, contact definitions prevent element penetration and simultaneously enable heat transfer between the interacting bodies, thereby replacing the free convection boundary condition. As the tool components are modeled as rigid bodies, these interactions result in the preform conforming to the cavity geometry while gradually cooling toward the tool temperature. Fig. 1 III illustrates the forming process, showing how the preheated preform is pressed into the cavity during tool closure. Once the tool is fully closed, the termination criterion for this simulation step is reached, thereby completing the first stage of the thermoforming simulation. Dividing the thermoforming simulation into discrete phases provides significant advantages. A restart capability allows the simulation to be resumed at any completed stage, facilitating efficient parameter studies. Furthermore, this approach enables the modification of all time- or temperature-dependent parameters individually within each simulation step.

Holding Time/Cooling Simulation.

In this simulation step, the holding phase is modeled, during which the tool remains closed either at a constant press force or at a constant gap, depending on the control strategy. During this phase, the preform gradually cools to the tool temperature. At present, no explicit crystallization kinetics are included; instead, the effects of crystallization on shrinkage and distortion are captured through the temperature-dependent, “crystallinity-adjusted” thermal expansion coefficient. More detailed models—such as Avrami, or Nakamura-type formulations-can be incorporated in future enhancements to account for the time- and temperature-dependent evolution of crystallinity and its influence on mechanical behavior. Care will be taken however to avoid excessive increases in simulation time, with the most computationally efficient models being tested first.

Spring-Angle Simulation.

In this simulation step, the tool is reopened after the prescribed holding time has elapsed. This is achieved by modifying the existing time-dependent smooth control curves in the restart file so that the two tool cavities return to their initial open positions. Once contact between the tool and the preform is fully released, the preform is again exposed to free convection with the surrounding air and continues to cool until it reaches ambient temperature. To prevent movement of the preform upon

removal from the tool, fixation boundary conditions are applied to selected nodes of the preform. These constraints restrict specific translational degrees of freedom while still allowing the component to deform freely. Through their connection to the remaining nodes, the three nodes with the minimum required translational constraints ensure that the preform maintains its central position within the tool. When selecting these nodes, only regions that experience minimal deformation during forming are considered. Nodes located in areas with radii or sharp edges are deliberately avoided to minimize their influence on the subsequent spring-in or spring-back behavior. Upon tool opening, the residual stresses accumulated within the preform become effective and induce deformation of the component, depending on their magnitude. This enables the spring-in and spring-back phenomena described previously to be captured within the simulation. The simulation results are evaluated using the post-processing tools provided by the LS-PrePost® software. For example, temperature and stress distributions can be visualized over time using iso-contours. In addition, angular changes -particularly at radii or inclined sections of the component - can be quantified as a function of time or position.

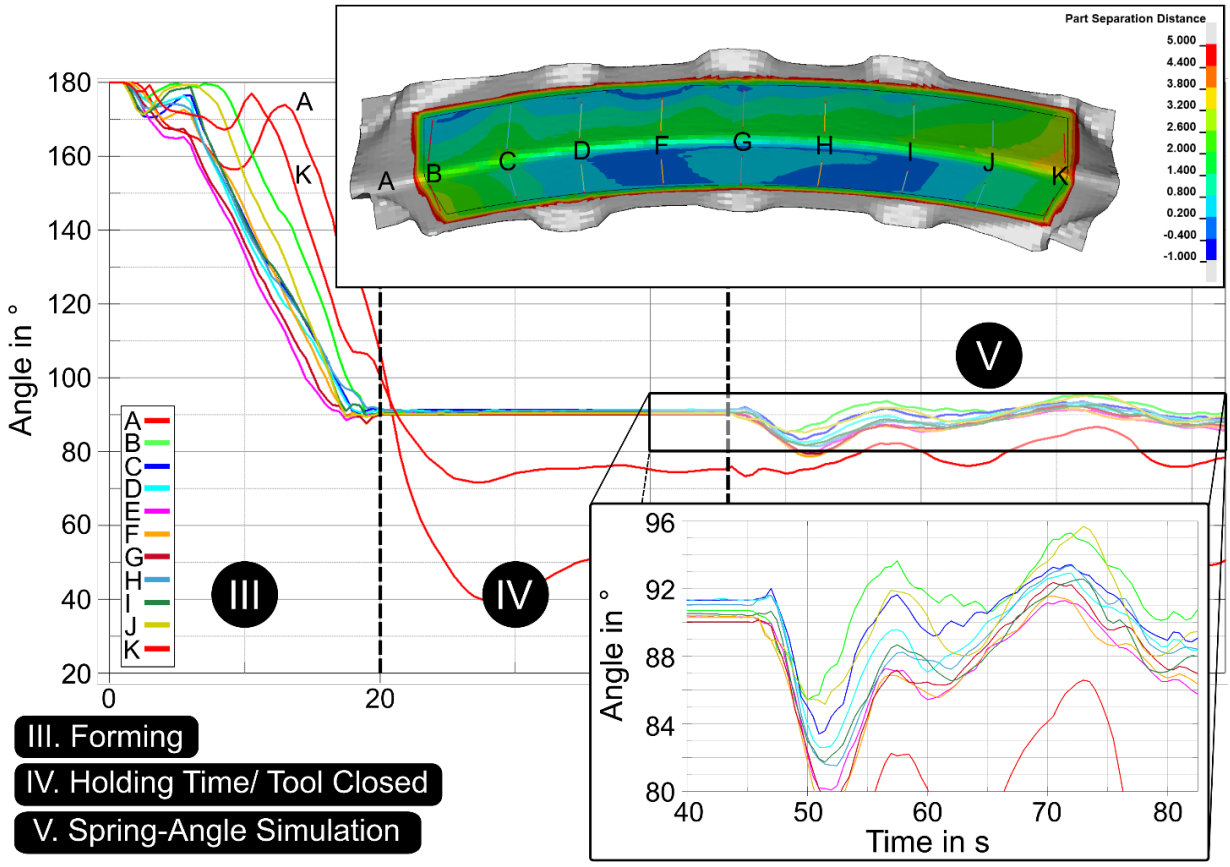

Fig. 4. Angular evolution of a thermoformed V-profile at several locations along the component length.

Fig. 4 illustrates the angular evolution of a thermoformed V-profile at several locations along the component length. The nominal enclosed angle is 90°. Throughout the simulation, the individual phases of the thermoforming process can be clearly distinguished. Starting from an initially flat preform (180°), the angles decrease during tool closure as a result of forming, reaching the target angle of 90° once the closing operation is completed. After the holding time and during tool opening, deviations from the nominal angle occur at the measurement locations due to residual stresses within the preform. In some cases, pronounced angular differences between individual measurement positions along the component length can be observed possibly resulting from the preform holding positions. Following partial stress relaxation through material deformation, a residual angular deviation remains relatively constant, the magnitude and direction of which depend on the specific application. Depending on whether the angle increases or decreases relative to the nominal value, the behavior is referred to as spring-back or spring-in, respectively.

Summary and Outlook

Using this modeling approach, the entire process chain - from preform manufacturing to thermoforming - can be simulated, providing systematic support for each individual process step. This enables substantial reductions in both time and cost during the planning and manufacturing of CFRTP components. In particular, preform generation can be efficiently supported by a simplified reverse thermoforming simulation, in which the target component geometry is used to derive a planar preform configuration. The thermoforming simulation itself provides early insight into the draping behavior and potential wrinkle/folding defect formation during the initial stages of forming. This allows corrective measures, such as preform post-processing through trimming operations, to be planned and implemented at an early stage. Following completion of the thermoforming simulation, the model enables prediction of component deformation caused by residual stresses introduced during forming. Based on these results, the press tool geometry can be adjusted to compensate for the simulated spring-in or spring-back effects.

A key advantage of this modeling approach is its high degree of flexibility and adaptability to a wide range of component geometries and process conditions. The modular structure of the overall model, combined with the unit-cell-based preform modeling strategy, enables flexible generation and exchange of preforms with arbitrary layup configurations, as well as efficient substitution of tool cavities and clamping frame concepts. The level of model complexity can be increased progressively as required. Fig. 5 illustrates several application cases to which the simulation methodology has already been successfully applied. These include simple geometries such as V-profiles, components of increased complexity such as profiles with closed edges, and highly complex double curvature geometries, for example S-shaped profiles combined with advanced clamping frame concepts. The primary limiting factors are the component geometry itself, which - analogous to real manufacturing conditions — must remain feasible to produce. In addition, increasing model size and complexity lead to a substantial rise in computational cost. As shown in Fig. 5, even relatively simple geometries currently require several days of computation on high-performance computing systems. Using a single computing node equipped with 32 AMD EPYC 9135 processors and the MPP (Massively Parallel Processing) version of the LS-DYNA solver, approximately 110 hours (4.5 days) are required to complete the entire simulation process chain for an axisymmetric v-shaped profile. This is despite the application of a thermal and gravity speed-up factor of 100, introduced specifically to reduce overall simulation times. Increasing this factor further leads to undesirable thermal and mechanical inertial effects and necessitates a reduction of the thermal and mechanical time steps, thereby eliminating any additional computational speed-up. In the most complex example shown in Figure 5, 24% of the total computational time is devoted to the thermoforming simulation phase, 44% to the holding phase, and the remaining 32% to the springback simulation phase. This distribution of computational effort among the different phases of the simulation remains largely consistent, irrespective of the specific part geometry. With further increases in model size and complexity, computation times may even extend to several weeks. However using several HPC cluster nodes (e.g. 512 or 1024 CPUs) can help decrease the computation time back to hours. Furthermore, the models enable unprecedented levels of detail and individual ply-level information.

In future work, additional process steps, such as overmolding and co-consolidation, may be incorporated into the simulations as subsequent stages within a single, unified simulation environment. This framework represents the complete process chain described above for the manufacturing of CFRTP components and is capable of predicting distortions arising throughout the entire thermoforming process.Owing to its high degree of adaptability, it can simulate a wide range of component geometries, providing effective support for both component development and

manufacturing process design. The simulation methodology will be validated by comparing predicted distortions with 3D scan measurements of the manufactured parts and their target CAD geometries.

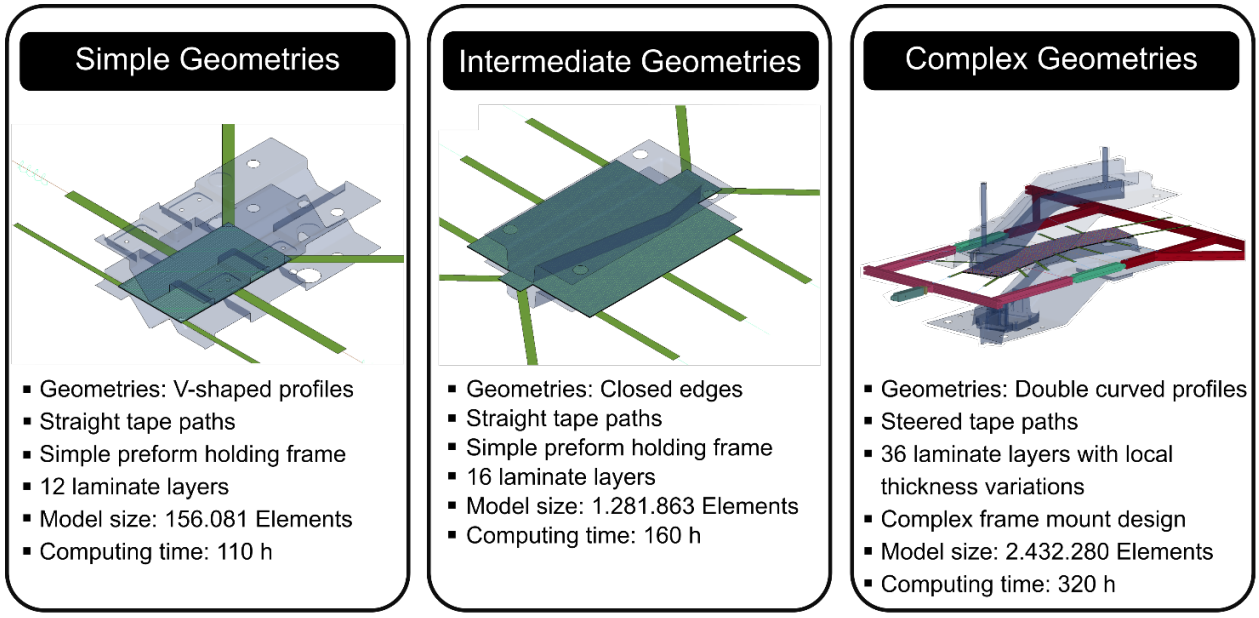

Fig. 5. Indication of model sizes and resulting simulation times (using 32 CPUs and MPP LS-DYNA® solver) for composite part geometries of various complexity.

Acknowledgement

The authors gratefully acknowledge the collaboration and R&D support provided by Aerospace Industrial Development Corporation (AIDC), Taiwan, in the development of the simulation technologies presented in this work. This work is also supported by the project *ZEUS – Zero Emission Aircraft with Sustainable Fuselage Concept and Technology*, funded by the Federal Ministry for Economic Affairs and Climate Action, following a decision of the German Bundestag (funding reference 20W2106F).

References

[1] M. Hou and K. Friedrich, "Stamp forming of continuous carbon fibre/polypropylene composites," *Compos. Manuf.*, vol. 2, no. 1, pp. 3–9, Mar. 1991, doi: 10.1016/0956-7143(91)90153-8.

[2] K. Friedrich and M. Hou, "Chapter 4 Thermoforming of continuous fibre/thermoplastic composite sheets," in *Composite Materials Series*, vol. 11, Elsevier, 1997, pp. 91–162. doi: 10.1016/S0927-0108(97)80006-9.

[3] N. Zahlan and J. M. O'Neill, "Design and fabrication of composite components; the spring-forward phenomenon," *Composites*, vol. 20, no. 1, pp. 77–81, Jan. 1989, doi: 10.1016/0010-4361(89)90685-X.

[4] M. Hou, K. Friedrich, and R. Scherer, "Optimization of stamp forming of thermoplastic composite bends," *Compos. Struct.*, vol. 27, no. 1, pp. 157–167, Jan. 1994, doi: 10.1016/0263-8223(94)90077-9.

[5] L. K. Jain, M. Hou, L. Ye, and Y.-W. Mai, "Spring-in study of the aileron rib manufactured from advanced thermoplastic composite," *Compos. Part Appl. Sci. Manuf.*, vol. 29, no. 8, pp. 973–979, Aug. 1998, doi: 10.1016/S1359-835X(97)00085-7.

[6] C. Albert and G. Fernlund, “Spring-in and warpage of angled composite laminates,” *Compos. Sci. Technol.*, vol. 62, no. 14, pp. 1895–1912, Nov. 2002, doi: 10.1016/S0266-3538(02)00105-7.

[7] R. B. Pipes, J. Hicks, E. Barocio, K. Chinwicharnam, and S. Yamamoto, “Shape compensation for carbon fiber thermoplastic composite stamp forming,” *Compos. Part B Eng.*, vol. 282, p. 111577, Aug. 2024, doi: 10.1016/j.compositesb.2024.111577.

[8] S.-W. Choi, M.-S. Lee, and C.-G. Kang, “Effect of process parameters and laminating methods on spring-back in V-bending of CFRP/CR340 hybrid composites,” *Int. J. Precis. Eng. Manuf.*, vol. 17, no. 3, pp. 395–400, Mar. 2016, doi: 10.1007/s12541-016-0049-1.

[9] Q. Miao, Z. Dai, G. Ma, F. Niu, and D. Wu, “Analysis of spring-back deformation of CF/PEEK thin angled laminates by laser-assisted forming,” *Compos. Struct.*, vol. 321, p. 117288, Oct. 2023, doi: 10.1016/j.compstruct.2023.117288.

[10] E. Hörberg, T. Nyman, M. Åkermo, and S. Hallström, “Thickness effect on spring-in of prepreg composite L-profiles – An experimental study,” *Compos. Struct.*, vol. 209, pp. 499–507, Feb. 2019, doi: 10.1016/j.compstruct.2018.10.090.

[11] Z. Padovec, V. Sháněl, M. Růžička, and N. Dolejš, “Java application for springback analysis of composite plates,” *Adv. Eng. Softw.*, vol. 72, pp. 77–84, Jun. 2014, doi: 10.1016/j.advengsoft.2013.06.003.

[12] G. C. Pereira, P. LeBoulluec, W.-T. Lu, M. I. Yoshida, A. P. Alves, and Antônio. F. Ávila, “Spring-back behavior on L-shaped composite structures: A statistical analysis of angular recovery as a function of time and residual cure,” *Compos. Part Appl. Sci. Manuf.*, vol. 124, p. 105491, Sep. 2019, doi: 10.1016/j.compositesa.2019.105491.

[13] D. Schommer, M. Duhovic, and J. Hausmann, “Modeling non-isothermal thermoforming of fabric- reinforced thermoplastic composites,” 2015.